Front. Optoelectron. 2021, 14(3): 311–320
https://doi.org/10.1007/s12200-020-1006-2

RESEARCH ARTICLE

Preparation of shape-controlling VO_2(M/R) nanoparticles via one-step hydrothermal synthesis

Yuchao LI[1,2], Fengyu KONG[3], Bin WANG[4], Yanhua ZHAO[2], Zuankai WANG (✉)[1,2]

1 Department of Mechanical Engineering, City University of Hong Kong, Hong Kong 999077, China
2 Shenzhen Research Institute of City University of Hong Kong, Shenzhen 518057, China
3 Ningbo University of Technology, Ningbo 315211, China
4 Shenzhen Institutes of Advanced Technology, Chinese Academy of Sciences, Shenzhen 518055, China

Abstract In this study, we developed a facile one-step hydrothermal process that allows to synthesize high-purity VO_2(M/R) nanoparticles with various morphologies such as nanorods, nanogranules, nanoblocks, and nanospheres. W dopants are successfully implanted in VO_2(M/R) unit cells with high doping efficiency, which allows to regulate the size, morphology, and phase of obtained nanoparticles. The underlying regulation mechanism is presented in detail to reveal how hydrothermal products vary with W doping contents, which provides a synthetic strategy for the preparation of shape-controlling VO_2(M/R) nanoparticles with high purity to satisfy different specific demands for corresponding applications in the field of thermochromic smart windows.

Keywords one-step hydrothermal, W doping, shape-controlling, VO_2(M/R) nanoparticles

1 Introduction

Vanadium dioxide (VO_2) is a typical thermochromic material, which has attracted extensive attention all over the world owing to its promising prospects in the fields of energy saving and emission reduction [1–3]. Though various types of VO_2 polymorphs have been developed, only the revisable crystallographic transformation between monoclinic VO_2(M) and tetragonal rutile VO_2(R) phases shows a 4–5 orders of magnitude change in resistivity and infrared transmittance at the critical transition temperature T_c of 68°C [4]. This unique metal–insulator transition (MIT) performance allows the material to be used as a switch to automatically control infrared (IR) transmission to regulate room temperature depending on the outer temperature; therefore, VO_2(M/R) is an ideal material for developing thermochromic smart windows [5].

During past decades, various types of technologies have been used to prepare high-purity VO_2(M/R). Among them, most methods in previous reports have mainly focused on the direct preparation of VO_2(M) film [6–8]. However, the process of synthesizing VO_2(M) nanoparticles first followed by the preparation of film using the as-obtained VO_2(M) nanoparticles is an equally important approach, but it has received less attention. Despite the comparatively complicated technical process, it can considerably decrease stress, which originates from the phase transition, to enhance lifespan. In addition, VO_2(M) nanoparticles can be mixed with other appropriate flexible organics to prepare VO_2(M) films with better optical performance under some specific conditions such as substrates with large area and special shapes [5]. Hence, it is still urgent and desirable to develop technology for the preparation of VO_2(M) nanoparticles.

Owing to the considerable efforts by numerous researchers, VO_2(M/R) nanoparticles have been successfully prepared by different methods such as wet chemistry [9], molten salt synthesis [10], pyrolysis [11], confined-space combustion [12], and hydrothermal synthesis [13–15]. Among them, hydrothermal synthesis is mostly used owing to its simplicity, comparatively environmentally friendly reaction conditions, and ability to control the grain growth.

Usually, the preparation of VO_2(M/R) nanoparticles through the hydrothermal synthesis process is separated into two steps: hydrothermal reaction and annealing treatment. In general, during the hydrothermal process, VO_2(B) nanobelts are generated as the mesophase and are ultimately transformed into VO_2(M/R) during the

Received January 11, 2020; accepted May 27, 2020

E-mail: zuanwang@cityu.edu.hk

subsequent annealing treatment. Then, the primitive nanostructures of VO_2(B) are nearly destroyed [16–18]. Nevertheless, one-step hydrothermal synthesis of VO_2(M/R), without annealing treatment, provides a possibility to prepare VO_2(M) nanoparticles by controlling morphology. Though various shapes for VO_2(M) nanoparticles have been presented in previous reports (e.g., nanorods [19], star-shaped nanoparticles [20], nanorings [21,22], nanoflowers [23], nanobeams [24], hollow spheres [25], and other shapes [26,27]), the shape-controlling mechanism still remains unclear, and there are only few reports that discuss it [28].

Herein, we reported a facile process through one-step hydrothermal synthesis to prepare high-purity VO_2(M/R) nanoparticles with various types of morphologies (e.g., nanorods, nanogranules, nanoblocks, and nanospheres) that can be well-regulated by different contents of W dopants implanted in VO_2 unit cells. In addition, we proposed a detailed possible explanation for the underlying shape regulation mechanism.

2 Experimental

2.1 Materials and characterization methods

All chemical agents (analytical grade purity) were obtained from J&K Scientific, Beijing and directly used as-received without further purification. Vanadium pentoxide (V_2O_5) served as the source of V atoms. Oxalic acid ($C_2H_2O_4 \cdot 2H_2O$) was used as the reductant. Ammonium (meta) tungstate hydrate, $(NH_4)_5H_5[H_2(WO_4)_6]$, was used as the source of W atoms. Ethyl alcohol (C_2H_5OH) and deionized water were used as solvents for the hydrothermal reaction.

The crystalline structure was characterized by X-ray diffraction (XRD) performed on a D8 discover (Bruker, USA) instrument with the Cu Kα radiation at a 40-kV accelerating voltage and 40-mA current. The size and morphology of nanoparticles were evaluated by field emission scanning microscopy (FESEM, JEOL, Japan). The elemental composition of samples was determined by an energy-dispersive X-ray spectroscopy (EDS) instrument coupled to FESEM. The chemical bonds of the samples were analyzed to confirm the oxidation state of vanadium using X-ray photoelectron spectroscopy (XPS, ESCA-Lab250Xi, Thermo Fisher Scientific, UK).

2.2 One-step hydrothermal synthesis of VO_2(M/R) nanoparticles

Figure 1 shows the schematic diagram of the one-step hydrothermal synthesis of VO_2 nanoparticles. In our experiment, 0.9455 g of $H_2C_2O_4$ was first dispersed into 37.5 mL of deionized water under magnetic stirring in a constant-temperature bath. After complete dissolution in 5 min, 0.6825 g of V_2O_5 powder was gradually added into the reaction solution to form a brick-red suspension, which could be uniformly dispersed in another 5 min. Subsequently, we used various contents of the

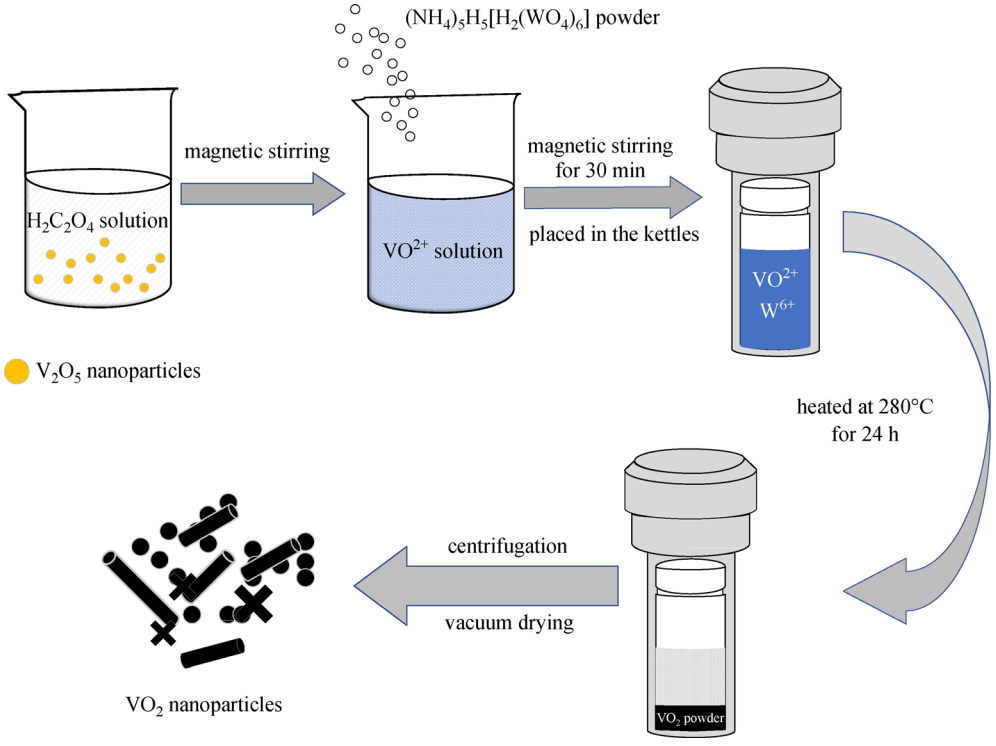

Fig. 1 Schematic diagram of the one-step hydrothermal synthesis of VO_2 nanoparticles

$(NH_4)_5H_5[H_2(WO_4)_6]$ powder for each group (see Table 1) to add into the mixed solution under vigorous stirring conditions. In the next 30 min, the suspended particles in the mixed solution were completely dissolved. Meanwhile, the suspension color became dark blue, which was the final precursor solution. Then, the precursor solution was carefully transferred into a 50-mL Teflon-lined reaction kettle with a stainless-steel shell. Then, the reaction kettle was heated at the temperature of 280°C for 24 h with a heating rate of 8°C/min, followed by natural furnace cooling until room temperature. Next, a dark blue precipitate was observed at the bottom of the kettle and separated from the solution by vacuum filtration. Subsequently, the precipitate was sequentially washed three times with deionized water, anhydrous alcohol, and deionized water. Finally, dark blue nanoparticles were obtained after centrifuging at 7000 r/min for 5 min and drying under vacuum at 60°C for 8 h.

3 Discussion

3.1 Doping efficiency of W atoms

In this section, we list the samples prepared with the W doping ratio of 1.0 at% as the value with the minimum W doping content set in our experiments. If W dopants are successfully demonstrated to be implanted into the end products for this group, it can also be applicable to other groups with a larger ratio because higher concentration indicates a stronger reaction rate.

Figures 2(a)–2(e) show EDS elemental mapping for the distribution of key elements in the prepared nanoparticles. It is determined that W dopants are uniformly distributed on the evaluated surface. Figure 2(f) shows the surface spectrogram in the range of 0–8 keV for VO_2 nanoparticles with the W doping ratio of 1.0 at% obtained by EDS coupled to FESEM. In addition to V and O elements, peaks for the W element are also detected at approximately 1.9, 2.1, and 8.4 keV, which confirm that W element has been successfully implanted into the final hydrothermal products.

Table 2 shows the difference between the nominal and W doping ratios. Table 2 shows that the real content of W in the final product is always lower than their corresponding theoretical values. In addition, the doping efficiency (ratio of the actual to nominal W doping ratios) is always less than 1, which also decreases with an increase in the W doping ratio (see Fig. 3). This occurs because the starting materials in hydrothermal reaction have their own different diffusion speeds. Consequently, there is always a portion of W element that is not capable of participating in the reaction. Even if the doping efficiency in our experiment is slightly lower than that in the previous research [29], VO_2 nanorods exhibit superior doping efficiency. However, such doping efficiency in our experiment is acceptable because our reaction time is only third compared to that in the abovementioned study. In the following section, to be convenient for the readers, we still use the data of nominal W doping ratio as the W doping ratio in this study.

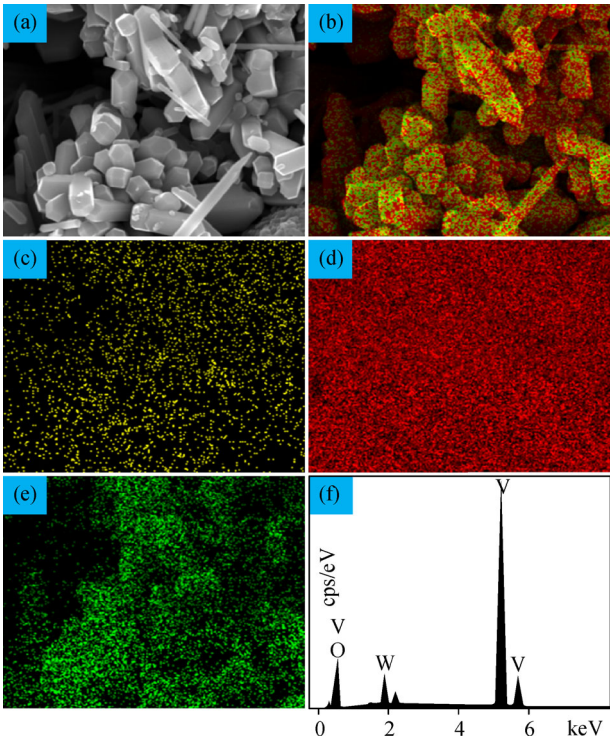

Fig. 2 Element mapping and surface spectrogram of VO_2 nanoparticles prepared with the W doping ratio of 1.0 at%. (a) SEM images of nanoparticles. (b) Overall diagram of the key elements: yellow color for W element, red color for O element, and green color for V element. (c) W element. (d) O element. (e) V element. (f) Surface spectrogram of different elements in the range of 0–8 keV. Here, cps is counts per second

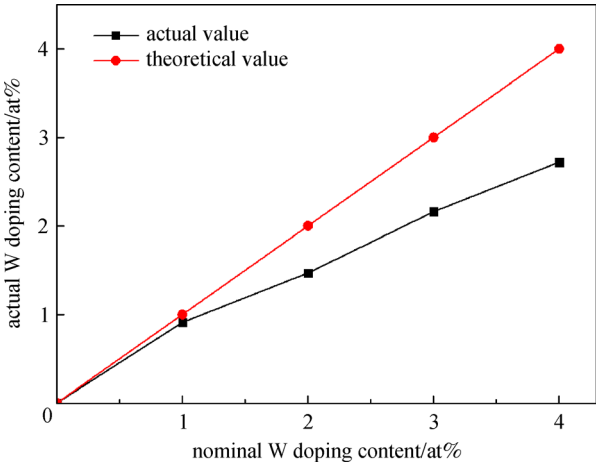

Fig. 3 Comparison of the nominal W and actual W doping content

Table 1 Contents of $(NH_4)_5H_5[H_2(WO_4)_6]$ powder for different groups

W doping ratio/at%*	weight/g
0	0
1.0	0.03758
2.0	0.07589
3.0	0.11274
4.0	0.15178

Note: * W doping ratio refers to the atomic percent of Watoms in the total of Wand V atoms in VO_2 crystals

3.2 Mechanism of phase evolution

During the hydrothermal synthesis of VO_2(M/R) with W dopants, the possible reaction can be characterized as follows. First, V_2O_5 particles are dispersed in oxidic acid, and V^{5+} is reduced to V^{4+}. The formula is shown in Eq. (1).

$$V_2O_5 + H_2C_2O_4 \rightarrow VOC_2O_4 + H_2O \quad (1)$$

In the precursor solution, VOC_2O_4 is a labile substance, which can be easily resolved into V^{4+}. Then, V^{4+} ions can further form the stabilized octahedral structure of the growth unit of $[VO_6]$. Then, $[VO_6]$ continues to develop into the new crystal nucleus at high temperature, which can grow into one-dimensional VO_2(B) for the following step. However, as an intermediate phase in the hydrothermal process, VO_2(B) is easily transformed into VO_2(M/R) at high temperature. Based on Leroux's research [30], the octahedral structure of $[VO_6]$ will be destroyed at first, and the connection between adjacent units of $[VO_6]$ will be also broken. Then, the obtained micro molecules regrow by elongating in two directions. Thus, the metaphase of VO_2(B) is transformed into VO_2(M). During the entire process, high temperature (generally, above 280°C) is necessary for the entire phase transition to obtain pure VO_2(M) [29].

W dopants are usually added to control the phase transition temperature between VO_2(M) and VO_2(R). In recent years, numerous studies have demonstrated that W dopants can not only regulate the morphology and size of as-obtained VO_2 nanoparticles but also facilitate the phase transition from VO_2(B) to VO_2(M). A possible explanation for the mechanism is that W^{6+} can replace V^{4+} in the unit cells of VO_2(B), which leads to lattice distortion owing to the larger ionic radius of W^{6+} (60 pm) compared to that of V^{4+} (58 pm). As a result, the connection between the adjacent units of $[VO_6]$ will break faster, giving rise to the rapid formation of VO_2(M/R). This observation provides a feasible method for the regulation of morphology, size, and purity of VO_2(M) by changing the content of W dopants added in the hydrothermal reaction. In our experiments, the source of W^{6+} is provided by ammonium metatungstate, which can be easily dissolved in water to generate W^{6+}, as shown in Eq. (2).

$$(NH_4)_5H_5[H_2(WO_4)_6] \rightarrow NH_3 + H_2O + H_2WO_4 \quad (2)$$

3.3 Phase behavior

Figure 4 shows XRD patterns of the hydrothermal reaction products prepared at 280°C for 24 h with different W doping ratios. For undoped VO_2, the phase of the end product is comprised of VO_2(B) and VO_2(M), which indicates that pure VO_2(M) cannot be obtained without W dopants in our experiments. However, when the W doping ratio increases to 1.0 at%, the end products are VO_2(M) nanoparticles with high purity because nearly all diffrac-

Table 2 Atomic percent of key elements in VO_2 nanoparticles determined by EDS

nominal W doping ratio/at%*	actual W doping ratio/at%*	elements	atom%	doping efficiency/%
0	0	O	64.33	0
		V	35.67	
		W	0	
1.0	0.91	O	66.74	91.0
		V	32.96	
		W	0.30	
2.0	1.47	O	63.82	73.5
		V	35.65	
		W	0.53	
3.0	2.16	O	65.36	72.0
		V	33.89	
		W	0.75	
4.0	2.72	O	64.74	68.0
		V	34.30	
		W	0.96	

Note: * Nominal W doping ratio refers to the atomic ratio of W atoms in the total of W and V atoms added to the mixture solution; actual W doping ratio refers to the atomic ratio of W atoms in the total of W and V atoms in the final products.

tion peaks are consistent with those of a standard VO_2(M) (JCPDS#43-1051) phase. When the W doping ratio is 2.0 at%, the end products are still pure VO_2(M) nanoparticles. Moreover, the intensity of peaks is also intensified compared to that of 1.0 at% doping ratio, which demonstrates a much higher crystallinity for the VO_2(M) crystal structure. Whereas, when the W doping ratio reaches 3.0 at%, the M(130) peak between 64° and 66° is split into R(310) and R(002) peaks (see Fig. 4), which is regarded as a diagnostic criterion for the phase transition from VO_2(M) to VO_2(R). It can be confirmed that the end product is a mixture of VO_2(M/R). However, minor impure peaks still appear at 29° despite of high purity of VO_2(M/R) nanoparticles. After the W doping ratio reaches 4.0 at%, except for the more obvious impure peaks, new impure peaks also appear at approximately 55°, which indicates that the purity of prepared VO_2(M/R) decreases. Overall, in our experiment, a certain amount of W dopants can facilitate the formation of VO_2(M) compared to nanoparticles prepared with the W doping ratio of 0, 1.0, and 2.0 at%. It can also promote the formation of VO_2(R) at the W doping ratio of 3.0 at%. However, excess amount of W dopants (4.0 at%) will lead to the generation of undesirable peaks during the hydrothermal reaction.

3.4 Morphological behavior

For undoped samples (see Fig. 5), the morphology of end products comprises hexagon nanoparticles with an average side length of 1.5 μm, aggregation bulk of multiple nanorods with an average length of 4 μm, and some snowflake nanoparticles (see Fig. 5(b)), which are mainly

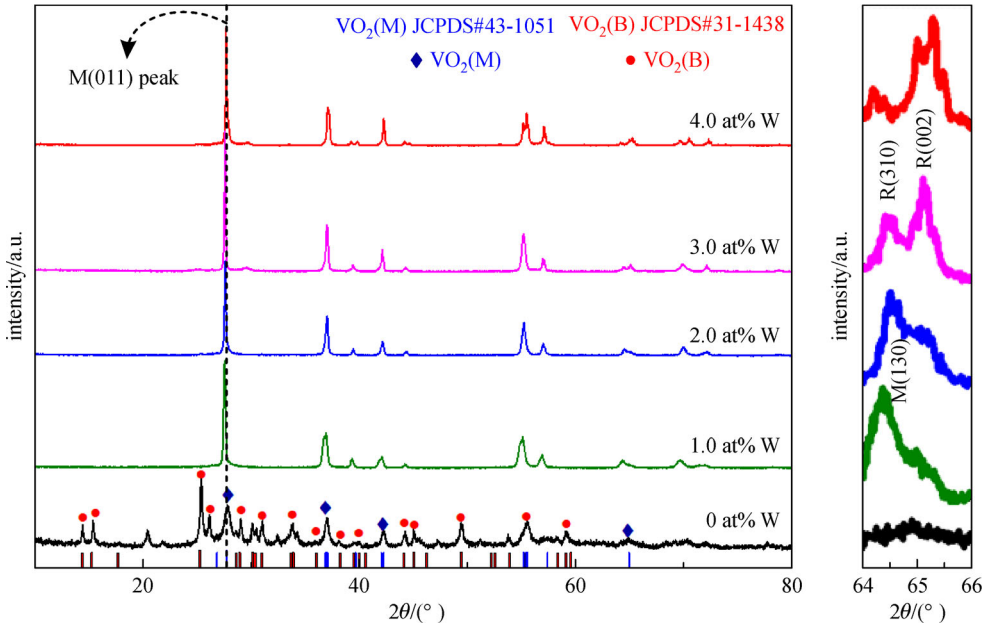

Fig. 4 XRD patterns of prepared nanoparticles with different W doping ratios (left) and a magnified view (right) of the XRD data in the range of $64° < 2\theta < 66°$

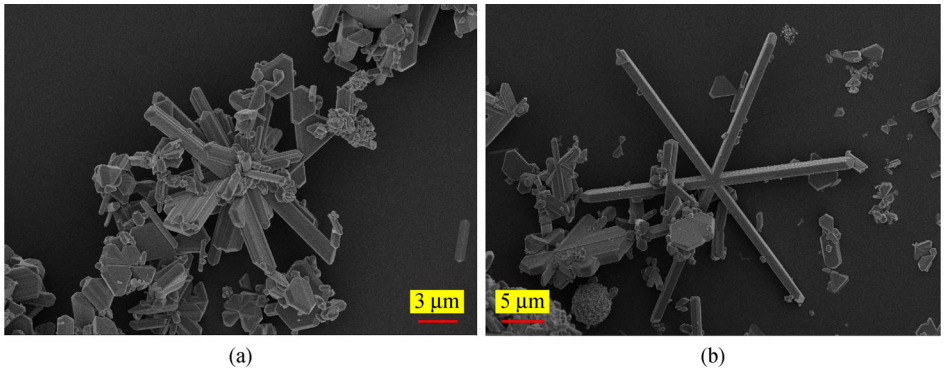

Fig. 5 SEM images of the prepared nanoparticles without W dopants. (a) Hexagon nanoparticles and nanorods. (b) Snowflake nanoparticles

caused by the preferable growth of the M(011) crystal facet. Combined with the analysis of XRD patterns in Fig. 4, there still exists a portion of VO_2(B) nanobelts, which has not been transformed into VO_2(M) nanoparticles without W dopants at 280°C for 24 h.

Figure 6 shows the morphology of nanoparticles prepared with the W doping ratio of 1.0 at%. The end products are a mixture of VO_2(M) nanogranules with an average diameter of 200 nm and VO_2(M) nanorods with an average length of 1 μm. Compared to undoped nanoparticles, the change in both phase and morphology is attributed to the replacement of a portion of V^{4+} in the VO_2 unit cell by W^{6+}. This change accelerates the decomposition of VO_2(B) owing to aggravated lattice distortion. Furthermore, the addition of W^{6+} brings extra electrons, which exist in d_{II} orbitals and can be transferred to adjacent V^{4+}. Thus, new chemical pairs of V^{3+}–W^{6+} and V^{3+}–V^{4+} are generated, which results in the formation of new oxygen vacancies of the unit cells. Consequently, the ability to incorporate surrounding elements is intensified, and the preferable growth of the M(011) peak is accelerated to generate nanorods with small size, which is confirmed by Fig. 4, where the M(011) peak becomes sharper when the W doping ratio changes from 0 to 3.0 at%.

To further confirm our explanation, we conducted XPS analysis of nanoparticles prepared with the W doping ratio of 1.0 at%, as shown in Fig. 7. Figure 7(a) shows the general patterns of the XPS spectrum, in which the peaks at 515–525 eV are attributed to V_{2p}, peaks at 35–42 eV are associated with W_{4f}, peak at 529.6 eV is associated with O_{1s}, peak at 631.5 eV is associated with V_{2s}, peak at 71.5 eV is associated with V_{3s}, and peaks at 43.2 eV and 700.0–850.5 eV are associated with V_{3p} and V (Auger), respectively. In addition, the peak at 516.5 eV is associated with $V_{2p3/2}$ (see Fig. 7(b)), which is below the reference value (517 eV) given for pure polycrystalline fully oxidized V_2O_5 [31] and demonstrates the existence of vanadium in low oxidation states (mainly V^{4+}). However, this value is higher than that of pure VO_2 in previous reports [32–36], which indicates that part of V^{4+} is reduced into V^{3+} during the exchange reaction [37]. In Fig. 7(c), the peaks at 35.6 eV and 37.6 eV are associated with $W_{4f7/2}$ and $W_{4f5/2}$, respectively, which demonstrates the existence of W^{6+} in VO_2 crystal cells. Therefore, our explanation for the regulation mechanism of W^{6+} is further confirmed. When the W doping ratio is 2.0 at%, nanoparticles completely disappear (see Fig. 8). Instead, only nanorods are present with an average length of 3 μm. More W^{6+} are implanted into VO_2 unit cells when more W^{6+} are added into the hydrothermal solution, which induces the generation of larger crystalline grains and accelerates the growth of VO_2(M).

Figure 9 shows nanoparticles prepared with the W doping ratio of 3.0 at%. Except for a portion of nanorods, most of them grew into massive nanoblocks with an average length of 700 nm. This result indicates that excess W^{6+}, which was implanted into VO_2 crystal cells, promotes lattice distortion and restrains the preferable growth of the M(001) crystal facet. This conclusion is further confirmed by the wider M(001) peaks in Fig. 4. Thus, massive nanoparticles with square and spherical shapes are generated. When the W doping ratio is increased to 4.0 at%, nanospheres are formed with an average diameter of 2 μm; these spheres are made of many nanoparticles with rough surfaces, as shown in Fig. 10. The lattice distortion of VO_2 crystal cells owing to the implantation of W^{6+} is further promoted, and the preferable growth of M(001) crystal facet is further restrained. Impure crystals are also observed in the end products.

Finally, the overall schematic diagram of the evolution of VO_2 nanoparticles and the regulation scheme based on different W doping contents is shown in Fig. 11. The morphologies of nanoparticles prepared in our experiment varied from nanogranules, nanorods, nanoblocks to nanospheres with an increase in the W doping content from 0 to 4.0 at%. In addition, we confirmed that W dopants can promote the phase transformation from VO_2(B) to VO_2(M), and the average size of as-obtained nanoparticles is increased from 200 nm to 2 μm with an increase in the W doping content.

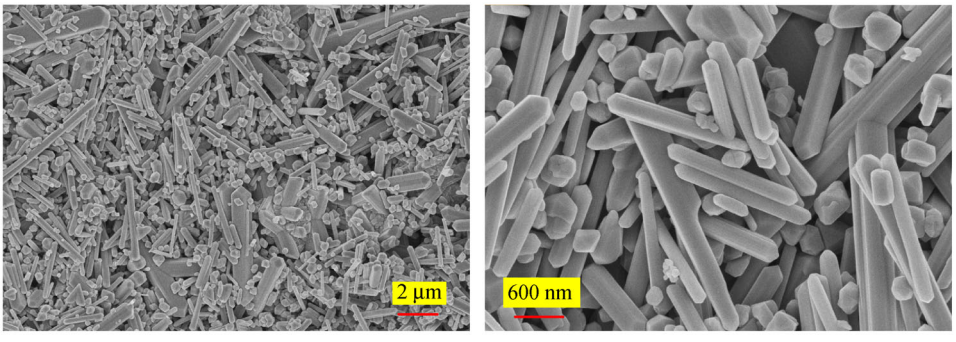

(a) (b)

Fig. 6 SEM images of prepared nanoparticles with the W doping ratio of 1.0 at% under different magnification. (a) ×5k. (b) ×20k

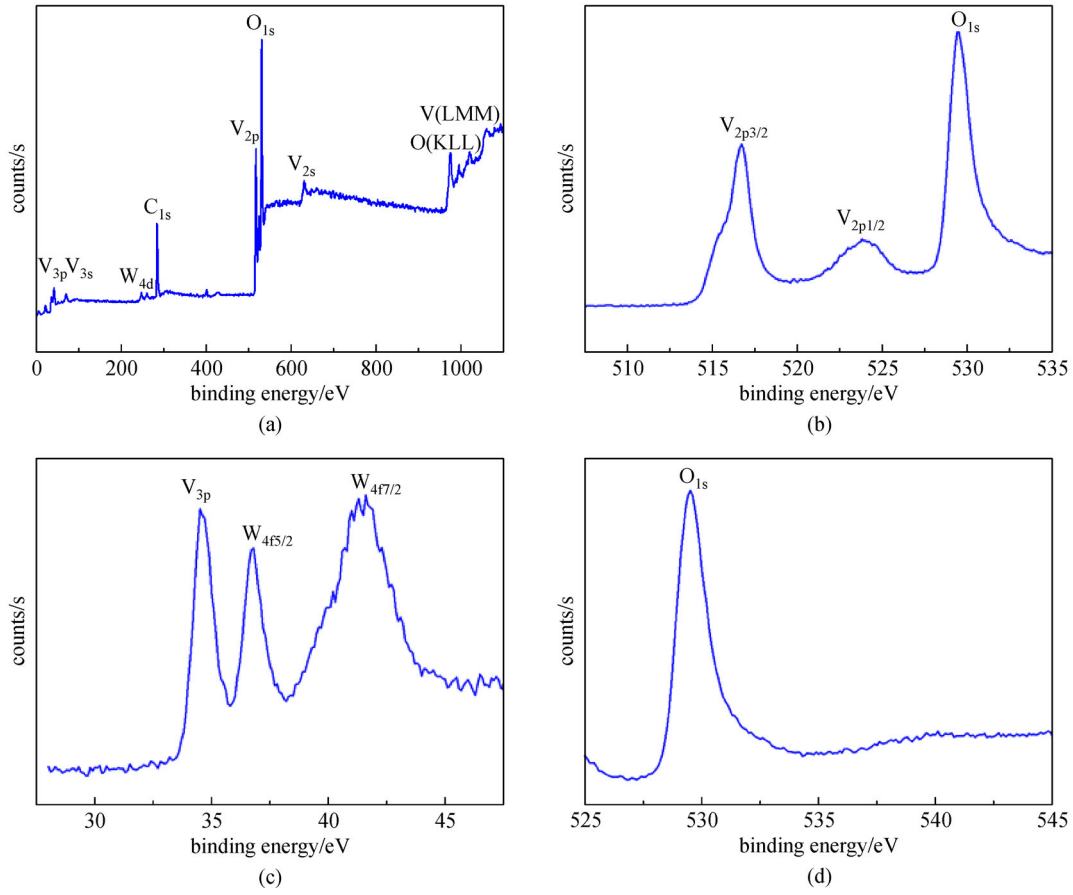

Fig. 7 XPS spectrum of nanoparticles prepared with the W doping ratio of 1.0 at%. (a) General patterns. (b) V element. (c) W element. (d) O element

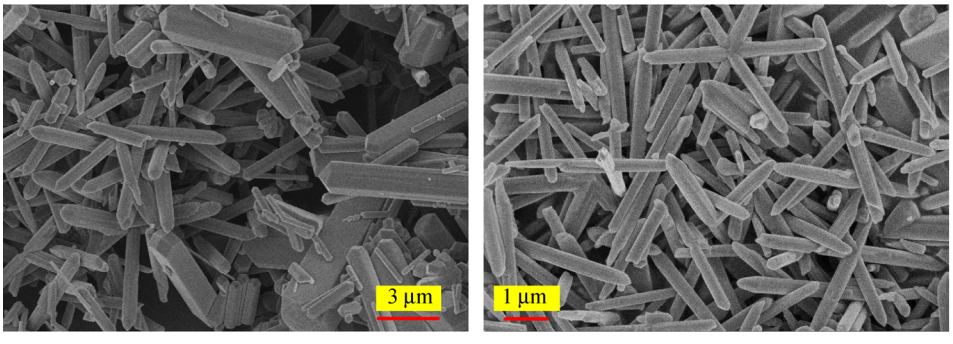

Fig. 8 SEM images of nanoparticles prepared with the W doping ratio of 2.0 at% under different magnification. (a) ×5k. (b) ×10k

4 Conclusions

In summary, we prepared high-purity VO_2(M/R) nanoparticles with various types of morphologies (e.g., nanogranules, nanorods, nanoblocks, and nanospheres) through one-step hydrothermal synthesis that is based on different W doping content. In our experiments, W dopants are essential in regulating the morphology of VO_2(M/R) nanoparticles through restraining the preferable growth of VO_2(M/R). In addition, we confirmed that a certain number of W dopants can promote the phase transformation from VO_2(B) to VO_2(M/R); however, excess content can lead to the generation of undesirable crystals and lower purity of nanoparticles. In general, our study provides a facile process by combining hydrothermal synthesis with W doping strategies to prepare high-purity shape-

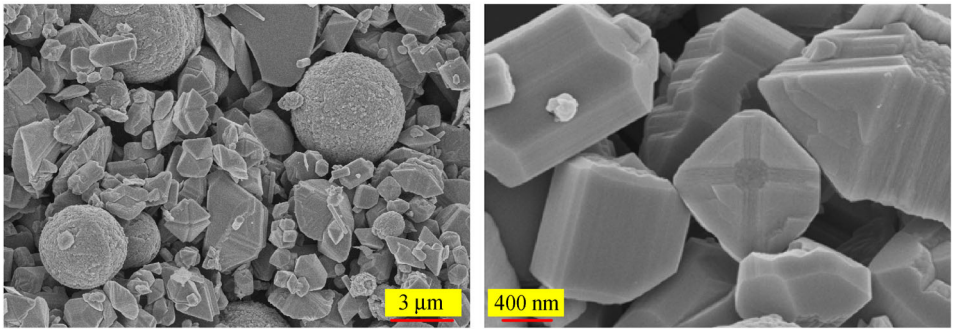

Fig. 9 SEM images of nanoparticles prepared with the W doping ratio of 3.0 at% under different magnification. (a) ×5k. (b) ×30k

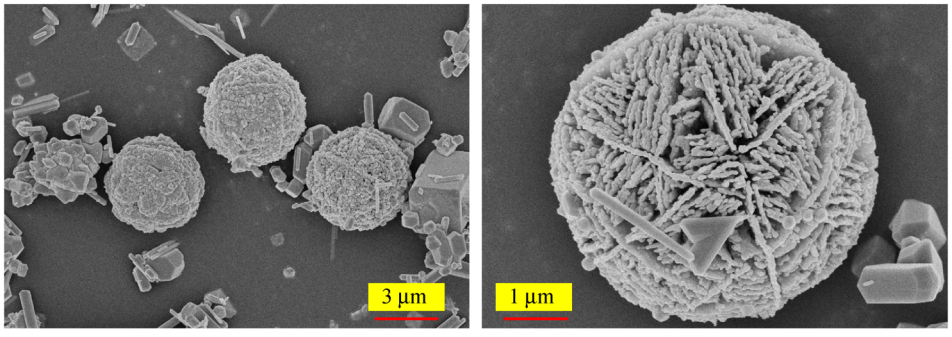

Fig. 10 SEM images of nanoparticles prepared with the W doping ratio of 4.0 at% under different magnification. (a) ×5k. (b) ×15k

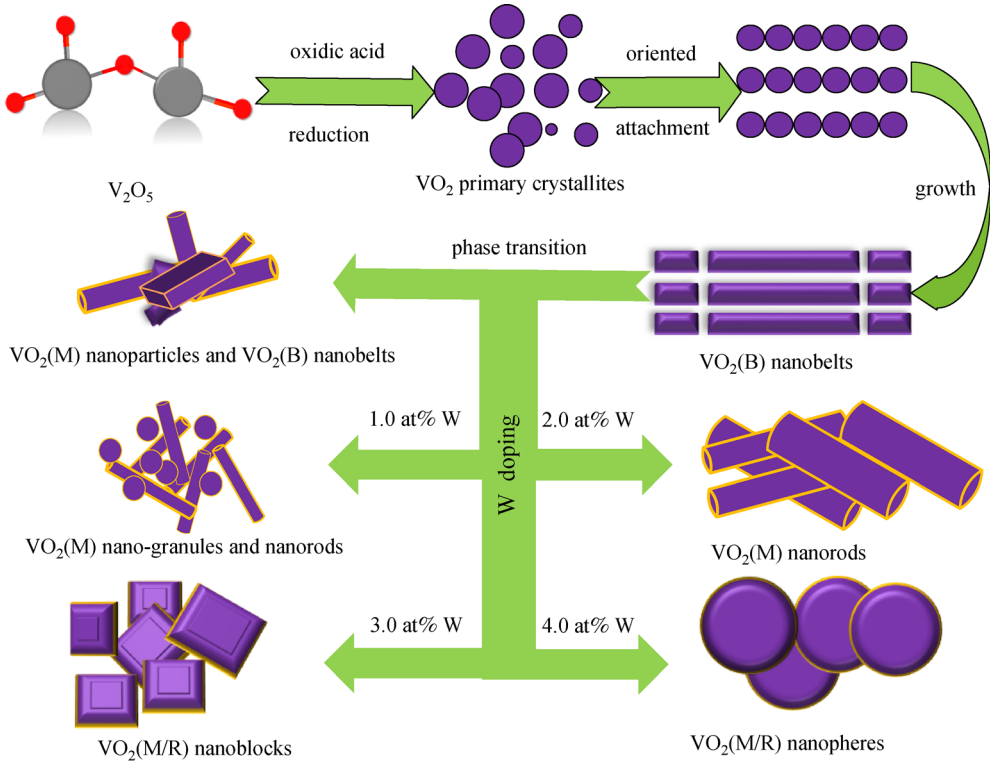

Fig. 11 Overall schematic diagram of evolution of VO_2 nanoparticles and regulation scheme

controlled VO_2(M/R) nanoparticles. This process is expected to be used in industrial mass production in the field of thermochromic smart windows because the process is simple, environmentally friendly, and allows to control the crystal growth. In addition, the approach used in this study to control the process of crystal growth with inorganic dopants to obtain shape-controlled nanoparticles can be also applied to the preparation of other metallic crystals to obtain desired morphologies.

Acknowledgements The authors acknowledge the financial support from the Shenzhen Science and Technology Innovation Council (No. JCYJ20170413141208098), the National Natural Science Foundation of China (Grant No. 51601101)

References

1. Corr S A, Grossman M, Furman J D, Melot B C, Cheetham A K, Heier K R, Seshadri R. Controlled reduction of vanadium oxide nanoscrolls: crystal structure, morphology, and electrical properties. Chemistry of Materials, 2008, 20(20): 6396–6404
2. Gao Y, Wang S, Kang L, Chen Z, Du J, Liu X, Luo H, Kanehira M. VO_2–Sb:SnO_2 composite thermochromic smart glass foil. Energy & Environmental Science, 2012, 5(8): 8234–8237
3. Wu C, Zhang X, Dai J, Yang J, Wu Z, Wei S, Xie Y. Direct hydrothermal synthesis of monoclinic VO_2(M) single-domain nanorods on large scale displaying magnetocaloric effect. Journal of Materials Chemistry, 2011, 21(12): 4509–4517
4. Paone A, Joly M, Sanjines R, Romanyuk A, Scartezzini J L, Schüler A. Thermochromic films of VO_2:W for smart solar energy applications. In: Proceedings of Optical Modeling and Measurements for Solar Energy Systems III. San Diego: International Society for Optics and Photonics, 2009, 7410: 74100F
5. Li M, Magdassi S, Gao Y, Long Y. Hydrothermal synthesis of VO_2 polymorphs: advantages, challenges and prospects for the application of energy efficient smart windows. Small, 2017, 13(36): 1701147
6. Xu Y, Huang W, Shi Q, Zhang Y, Wu J, Song L. Porous nanostructured VO_2 films with different surfactants: synthesis mechanisms, characterization, and applications. Journal of Materials Science Materials in Electronics, 2013, 24(10): 3823–3829
7. Taha M, Walia S, Ahmed T, Headland D, Withayachumnankul W, Sriram S, Bhaskaran M. Insulator–metal transition in substrate-independent VO_2 thin film for phase-change devices. Scientific Reports, 2017, 7(1): 17899
8. Zhang Z, Gao Y, Chen Z, Du J, Cao C, Kang L, Luo H. Thermochromic VO_2 thin films: solution-based processing, improved optical properties, and lowered phase transformation temperature. Langmuir, 2010, 26(13): 10738–10744
9. Li S, Li Y, Jiang M, Ji S, Luo H, Gao Y, Jin P. Preparation and characterization of self-supporting thermochromic films composed of VO_2(M)@SiO_2 nanofibers. ACS Applied Materials & Interfaces, 2013, 5(14): 6453–6457
10. Wang F, Liu Y, Liu C Y. Molten salt synthesis and localized surface plasmon resonance study of vanadium dioxide nanopowders. Journal of Solid State Chemistry, 2009, 182(12): 3249–3253
11. Zheng C, Zhang X, Zhang J, Liao K. Preparation and characterization of VO_2 nanopowders. Journal of Solid State Chemistry, 2001, 156(2): 274–280
12. Wu C, Dai J, Zhang X, Yang J, Qi F, Gao C, Xie Y. Direct confined-space combustion forming monoclinic vanadium dioxides. Angewandte Chemie International Edition, 2010, 49(1): 134–137
13. Cao C, Gao Y, Luo H. Pure single-crystal rutile vanadium dioxide powders: synthesis, mechanism and phase-transformation property. Journal of Physical Chemistry C, 2008, 112(48): 18810–18814
14. Son J H, Wei J, Cobden D, Cao G Z, Xia Y N. Hydrothermal synthesis of monoclinic VO_2 micro-and nanocrystals in one step and their use in fabricating inverse opals. Chemistry of Materials, 2010, 22(10): 3043–3050
15. Whittaker L, Jaye C, Fu Z, Fischer D A, Banerjee S. Depressed phase transition in solution-grown VO_2 nanostructures. Journal of the American Chemical Society, 2009, 131(25): 8884–8894
16. Zhang K F, Liu X, Su Z X, Li H L. VO_2(R) nanobelts resulting from the irreversible transformation of VO_2(B) nanobelts. Materials Letters, 2007, 61(13): 2644–2647
17. Kam K C, Cheetham A K. Thermochromic VO_2 nanorods and other vanadium oxides nanostructures. Materials Research Bulletin, 2006, 41(5): 1015–1021
18. Li J, Liu C, Mao L. The character of W-doped one-dimensional VO_2(M). Journal of Solid State Chemistry, 2009, 182(10): 2835–2839
19. Gui Z, Fan R, Mo W, Chen X, Yang L, Zhang S, Hu Y, Wang Z, Fan W. Precursor morphology controlled formation of rutile VO_2 nanorods and their self-assembled structure. Chemistry of Materials, 2002, 14(12): 5053–5056
20. Alie D, Gedvilas L, Wang Z, Tenent R, Engtrakul C, Yan Y, Shaheen S E, Dillon A C, Ban C. Direct synthesis of thermochromic VO_2 through hydrothermal reaction. Journal of Solid State Chemistry, 2014, 212: 237–241
21. Li M, Kong F, Zhang Y, Li G. Hydrothermal synthesis of VO_2(B) nanorings with inorganic V_2O_5 sol. Royal Society of Chemistry, 2011, 13(7): 2204–2207
22. Dong Y, Li S, Zhao K, Han C, Chen W, Wang B, Wang L, Xu B, Wei Q, Zhang L, Xu X, Mai L. Hierarchical zigzag $Na_{1.25}V_3O_8$ nanowires with topotactically encoded superior performance for sodium-ion battery cathodes. Energy & Environmental Science, 2015, 8(4): 1267–1275
23. Zhang S, Li Y, Wu C, Zheng F, Xie Y. Novel flowerlike metastable vanadium dioxide (B) micronanostructures: facile synthesis and application in aqueous lithium ion batteries. Journal of Physical Chemistry C, 2009, 113(33): 15058–15067
24. Wang N, Duchamp M, Xue C, Dunin-Borkowski R E, Liu G, Long Y. Single-crystalline W-doped VO_2 nanobeams with highly reversible electrical and plasmonic responses near room temperature. Advanced Materials Interfaces, 2016, 3(15): 1600164
25. Liu H, Wang Y, Wang K, Hosono E, Zhou H. Design and synthesis of a novel nanothorn VO_2(B) hollow microsphere and their application in lithium-ion batteries. Journal of Materials Chemistry, 2009, 19(18): 2835–2840
26. Dai L, Chen S, Liu J, Gao Y, Zhou J, Chen Z, Cao C, Luo H, Kanehira M. F-doped VO_2 nanoparticles for thermochromic

energy-saving foils with modified color and enhanced solar-heat shielding ability. Physical Chemistry Chemical Physics, 2013, 15 (28): 11723–11729
27. Zhou J, Gao Y, Liu X, Chen Z, Dai L, Cao C, Luo H, Kanahira M, Sun C, Yan L. Mg-doped VO_2 nanoparticles: hydrothermal synthesis, enhanced visible transmittance and decreased metal-insulator transition temperature. Physical Chemistry Chemical Physics, 2013, 15(20): 7505–7511
28. Chen R, Miao L, Liu C, Zhou J, Cheng H, Asaka T, Iwamoto Y, Tanemura S. Shape-controlled synthesis and influence of W doping and oxygen nonstoichiometry on the phase transition of VO_2. Scientific Reports, 2015, 5(1): 14087
29. Chen R, Miao L, Cheng H, Nishibori E, Liu C, Asaka T, Iwamoto Y, Takata M, Tanemura S. One-step hydrothermal synthesis of $V_{1-x}W_xO_2$(M/R) nanorods with superior doping efficiency and thermochromic properties. Journal of Materials Chemistry A, Materials for Energy and Sustainability, 2015, 3(7): 3726–3738
30. Leroux C, Nihoul G, Tendeloo G V. From VO_2(B), to VO_2(R): theoretical structures of VO_2, polymorphs and *in situ*, electron microscopy. Physical Review B, 1998, 57(9): 5111–5121
31. Wagner C D, Riggs W M, Davis L E, Moulder J F, Muilenberg G E. Handbook of X-ray Photoelectron Spectroscopy. Minnesota: Perkin-Elmer Corporation Press, 1979, 38
32. Kurmaev E Z, Cherkashenko V M, Yarmoshenko Y M, Bartkowski S, Postnikov A V, Neumann M, Duda L C, Guo J H, Nordgren J, Perelyaev V A, Reichelt W. Electronic structure of studied by X-ray photoelectron and X-ray emission spectroscopies. Journal of Physics Condensed Matter, 1998, 10(18): 4081–4091
33. Cui J, Da D, Jiang W. Structure characterization of vanadium oxide thin films prepared by magnetron sputtering methods. Applied Surface Science, 1998, 133(3): 225–229
34. Yin D, Xu N, Zhang J, Zheng X. High quality vanadium dioxide films prepared by an inorganic sol-gel method. Materials Research Bulletin, 1996, 31(3): 335–340
35. Burkhardt W, Christmann T, Meyer B K, Niessner W, Schalch D, Scharmann A. W- and F-doped VO_2 films studied by photoelectron spectrometry. Thin Solid Films, 1999, 345(2): 229–235
36. Lu S, Hou L, Gan F. Surface analysis and phase transition of gel-derived VO_2 thin films. Thin Solid Films, 1999, 353(1–2): 40–44
37. Li F, Wang X, Shao C, Tan R, Liu Y. W doped vanadium oxide nanotubes: synthesis and characterization. Materials Letters, 2007, 61(6): 1328–1332

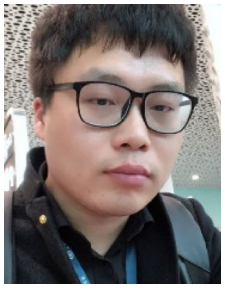

Yuchao Li received his B.S. and M.D. degrees from Tongji University and Shandong University, China in 2014 and 2018, respectively. He now is a Ph.D. student at City University of Hong Kong, China supervised by Prof. Zuankai Wang. His current research is focused on the design and characterization of thermochromic materials, electrowetting and nanogenerators.

E-mail: yuchaoli3-c@my.cityu.edu.hk

Fengyu Kong is an assistant professor in Department of Materials and Chemical Engineering at Ningbo University of Technology, China. She was also a senior research assistant in Department of Mechanical Engineering at City University of Hong Kong, China, in 2017. She received her Ph.D. degree in Condensed Matter Physics from Institute of Solid State Physics, Chinese Academy of Sciences, China, in 2012, and B.S. degree in Materials Science and Engineering from China University of Geosciences, China, in 2007. Her current research is focused on design and modification of functional metal oxide and amorphous-nanocrystalline alloy, especially in the intelligent energy saving field.

E-mail: fengyu.k@hotmail.com

Bin Wang is now an associated professor at Shenzhen Institutes of Advanced Technology, Chinese Academy of Sciences, China. She received her Ph.D. degree from University of California, San Diego, USA, in 2016. Dr. Wang's research focuses on the design and manufacturing of advanced, hierarchically structured materials.

E-mail: bin.wang@siat.ac.cn

Yanhua Zhao is now a postdoctoral fellow supervised by Prof. Zuankai Wang at City University of Hong Kong, China. She also received her Ph.D. degree from City University of Hong Kong, China. Dr. Zhao's research focuses on the design and manufacturing of bionically hierarchically structured materials.

E-mail: yanhuzhao3-c@my.cityu.edu.hk

Zuankai Wang is a professor in Department of Mechanical Engineering at City University of Hong Kong, China. He received his Ph.D. degree in Mechanical Engineering from Rensselaer Polytechnic Institute, USA, in 2008, his M.S. degree in Microelectronics from Shanghai Institute of Microsystem and Information Technology, Chinese Academy of Sciences, China, in 2003, and B.S. degree in Mechanical Engineering from Jilin University, China, in 2000. His current research is focused on the fundamental understanding of basic structure–function properties of natural materials as well as applying nature's inspiration for the development of novel interfacial materials and devices.

E-mail: zuanwang@cityu.edu.hk